

# A Sensitive Phenol Electrochemical Sensor Based on Magnetic Oxide/Amino-Functional Graphene Nanocomposite

Zuchao Meng\*, Mao Li, Chengxi Li, Xiang Liu, Zigang Lei

College of Chemistry and Chemical Engineering, Xi'an shiyou University, Xi'an Shaanxi 710065, China

\*E-mail: [zcmeng@xsysu.edu.cn](mailto:zcmeng@xsysu.edu.cn)

Received: 20 January 2018 / Accepted: 12 December 2018 / Published: 7 February 2019

A sensitive electrochemical sensor for the detection of phenol was fabricated based on a magnetic oxide/amino-functionalized graphene ( $\text{Fe}_3\text{O}_4/\text{AGO}$ ) nanocomposite.  $\text{Fe}_3\text{O}_4/\text{AGO}$  was synthesized by chemical coprecipitation. The morphologies and structures of  $\text{Fe}_3\text{O}_4/\text{AGO}$  were studied with a scanning electron microscope (SEM), transmission electron microscope (TEM), Fourier transform infrared spectroscope (FTIR) and X-ray diffractometer (XRD). The effects of the pH and scan rate on the electrocatalytical oxidation of phenol were also investigated. Under the optimized conditions, the oxidation peak currents were proportional to the phenol concentrations in the ranges of  $0.45 \mu\text{M} \sim 56 \mu\text{M}$  and  $156 \mu\text{M} \sim 456 \mu\text{M}$  with a lower detection limit of  $0.4 \mu\text{M}$  ( $S/N=3$ ). Furthermore, the fabricated sensor was successfully applied to the detection of phenol in an oilfield wastewater sample with satisfactory results.

**Keywords:**  $\text{Fe}_3\text{O}_4$  magnetic nanoparticle, amino-functional graphene, phenol, sensor

## 1. INTRODUCTION

As a protoplasmic toxin with strong toxicity, phenol exists widely in coking wastewater, pesticides, and the petroleum chemical industry and can cause serious pollution of the land and water ecological systems, directly endangering human health and aquatic life. Therefore, the detection of phenol in the environment is very important for maintaining a clean environment. At present, various methods have been employed for the determination of phenol, including gas chromatography[1], high-performance liquid chromatography[2], flow-injection spectrophotometry[3], capillary electrophoresis [4], spectrophotometry[5] and electrochemical methods [6-8]. However, most of the above methods involve time-consuming and cumbersome procedures. Electrochemical methods have been widely used for the detection of phenol due to their rapid response, low cost and ease of use[9-10].

Owing to its large specific surface area, biocompatibility, excellent electrocatalytic activity, fast electron transfer, strong mechanical strength and high chemical stability, graphene has been wildly used. At present, many electrochemical sensors, including ascorbic acid[11], nitrite[12], lead and cadmium[13], colorants[14] and biosensors[15], have been fabricated based on graphene. In addition, as a two-dimensional material, both sides of graphene can be used to support the catalysts[16]. Magnetic Fe<sub>3</sub>O<sub>4</sub> nanoparticles have been widely used in magnetic resonance imaging, drug delivery, biological separation, and biocatalysis[17-19]. Due to their low toxicity and good biocompatibility in physiological environments, Fe<sub>3</sub>O<sub>4</sub> nanomaterials have been given more attention as electrochemical sensors and biosensors, such as for use in lead analysis[20], H<sub>2</sub>O<sub>2</sub> analysis[21], and immunoassays[22].

To the best of our knowledge, the use of a Fe<sub>3</sub>O<sub>4</sub>/AGO nanocomposite as a sensor for the detection of phenol has not been reported previously. In this work, a highly sensitive phenol electrochemical sensor based on a Fe<sub>3</sub>O<sub>4</sub>/AGO nanocomposite is presented, which was successfully used to determine the phenol content in oilfield wastewater.

## 2. EXPERIMENTAL

### 2.1 Chemical and reagents

Phenol was purchased from Tianjin Fuchen Chemical Reagents Factory (Tianjin, China). Graphite powder was obtained from the Guoyao Group of Chemical Reagent Co. Ltd. concentrated sulfuric acid (H<sub>2</sub>SO<sub>4</sub>) and hydrogen peroxide (H<sub>2</sub>O<sub>2</sub>) were purchased from Sichuan Xilong Chemical Co. Ltd. Sodium nitrate (NaNO<sub>3</sub>), potassium permanganate (KMnO<sub>4</sub>) and sodium hydroxide (NaOH) were obtained from Tianjin Kermel Chemical Reagent Co. Ltd. Hexahydrate ferric chloride (FeCl<sub>3</sub>·6H<sub>2</sub>O) was purchased from Crystal Shifu Chen Chemical Reagent, heptahydrate ferrous sulfate (FeSO<sub>4</sub>·7H<sub>2</sub>O) was purchased from Xi'an Chemical Reagent, concentrated ammonia (NH<sub>3</sub>·H<sub>2</sub>O) was purchased from Zhengzhou Piney Chemical Reagent, and ethanol was purchased from Tianjin Tianli Chemical Co. Ltd. All of the above materials are analytical reagents. The oilfield wastewater was collected from the Changqing Oil Production Plant. Phosphate buffered saline solutions (PBS) (0.1 M) with different pH values were prepared by mixing stock standard solutions of K<sub>2</sub>HPO<sub>4</sub> and KH<sub>2</sub>PO<sub>4</sub> and adjusting the pH with either 0.1 M H<sub>3</sub>PO<sub>4</sub> or KOH. All of the solutions were prepared with doubly distilled water.

### 2.2 Apparatus

A model CHI660A Electrochemistry Workstation (Chenhua Instruments Co. Ltd., Shanghai, China) was employed for all of the electrochemical techniques. A three-electrode system was used, where a standard saturated calomel electrode (SCE) served as the reference electrode, a platinum wire electrode served as the auxiliary electrode, and a modified glassy carbon electrode served as the working electrode. All of the electrochemical experiments were conducted at room temperature (25 °C).

Scanning electron microscopy(SEM) and energy dispersive spectroscopy (EDS) were measured

on a JSM-6700F scanning electron microscope (Japan Electronics Corporation, Japan). Transmission electron microscopy(TEM) was recorded on a transmission electron microscope (Tecnai G2F20 S-Twin, FEI, USA). X-ray diffraction (XRD) was recorded by an X-ray diffractometer (Ricoh Corporation, Tokyo, Japan).

### 2.3 Preparation of graphite oxide

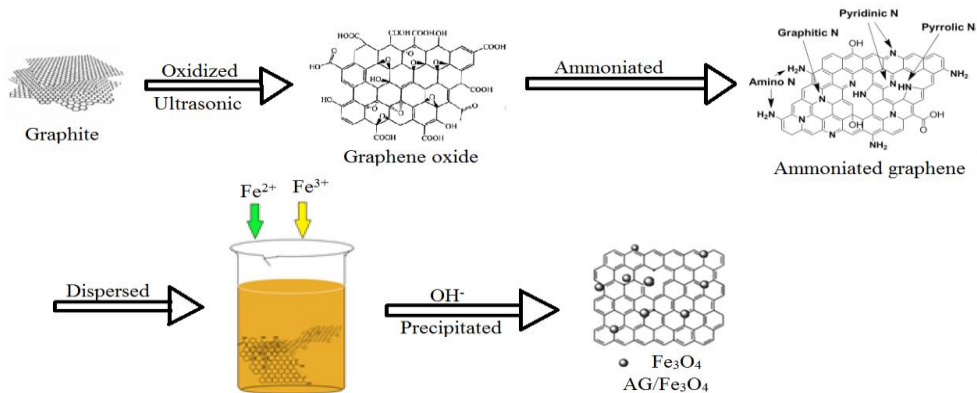
Graphite oxide was prepared from purified natural graphite according to Hummer's method [23-24]. In detail, graphite powder and NaNO<sub>3</sub> were added to concentrated H<sub>2</sub>SO<sub>4</sub> (120 mL) in an ice bath for 15 min with stirring at temperatures below 10 °C. Then, KMnO<sub>4</sub> (20 g) was slowly added to the mixture and maintained at temperature for 35 min. Then, the reaction was transferred to a 40 °C water bath for 75 min. Upon completion of the reaction, deionized water was added slowly at 98 °C for 5 min and vigorously stirred. The mixture was treated with a solution of 30% H<sub>2</sub>O<sub>2</sub>. The above mixture was allowed to settle to collect the bottom layer. The product was washed repeatedly with a solution of 5% HCl. Finally, the material was dried at 60 °C for 12 h, and graphite oxide was obtained.

### 2.4 The preparation of AGO

AGO was synthesized according to the literature[25]. In a typical procedure, graphite oxide was added to 10 mL of water and sonicated for 0.5 h. Next, 70 mL of an ammonia solution (25 wt% in water) was added, and the mixture was poured into a 100 mL Teflon-lined autoclave and kept at 200 °C for 12 h. The resulting black solid was washed with a 5% HCl solution to remove the remaining ammonia solution. AGO could then be obtained by filtration and drying at 60 °C for 12 h.

### 2.5 The preparation of the Fe<sub>3</sub>O<sub>4</sub>/AGO nanocomposite

The preparation process is shown in Scheme 1. After 232 mg of AGO was dispersed in 200 mL of deionized water under sonication, the mixture was transferred into a four-port flask and sonicated for 1 h to obtain a homogeneous dispersion. An aqueous solution of 1.4 g FeSO<sub>4</sub>•7H<sub>2</sub>O and 2.7 g FeCl<sub>3</sub>•6H<sub>2</sub>O was transferred into the flask under sonication. The mixture was heated to 60 °C in a water bath, and 1.6 g of a NaOH solution was added rapidly into the flask. After the mixture was stirred at 60°C for 2 h, the mixture was dried at 60 °C for 12 h, and the Fe<sub>3</sub>O<sub>4</sub>/AGO composite was obtained through grinding.



**Scheme 1.** Scheme of the preparation of Fe<sub>3</sub>O<sub>4</sub>/AGO composite

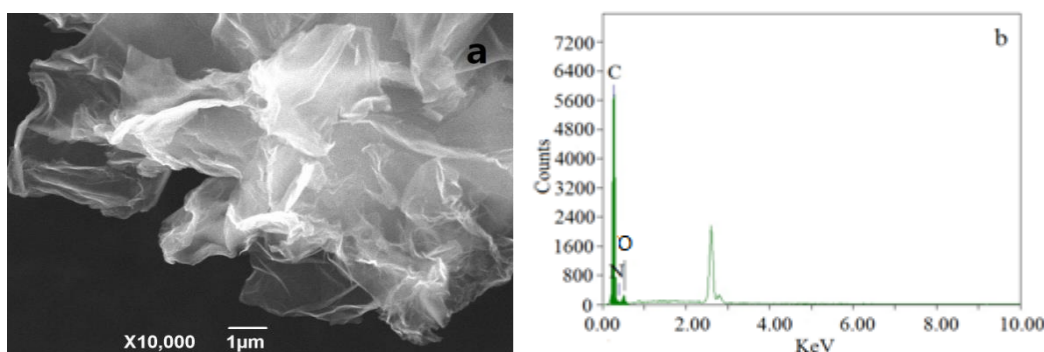
### 2.6 Preparation of the Fe<sub>3</sub>O<sub>4</sub>/AGO/GCE

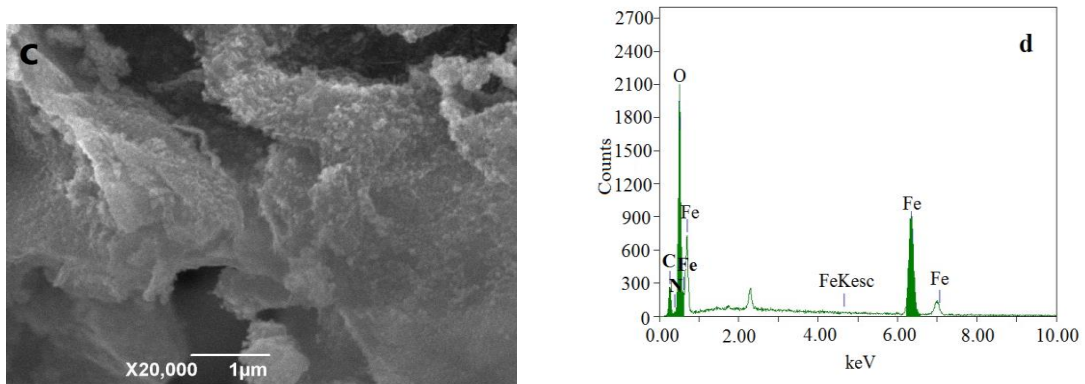
The bare GCE was polished to a mirror-like surface with 1.0, 0.3, and 0.05 µm α-Al<sub>2</sub>O<sub>3</sub>, sequentially. After the cleaned electrode was dried, 10 µL of a 3 mg/mL Fe<sub>3</sub>O<sub>4</sub>/AGO suspension was dropped onto the surface of the GCE. After drying in air, the Fe<sub>3</sub>O<sub>4</sub>/AGO-modified GCE (Fe<sub>3</sub>O<sub>4</sub>/AGO/GCE) was obtained. For comparison, Fe<sub>3</sub>O<sub>4</sub>/GCE and AGO/GCE were prepared by replacing Fe<sub>3</sub>O<sub>4</sub>/AGO with either Fe<sub>3</sub>O<sub>4</sub> or AGO.

## 3. RESULTS AND DISCUSSION

### 3.1 Characterization of the Fe<sub>3</sub>O<sub>4</sub>/AGO composite

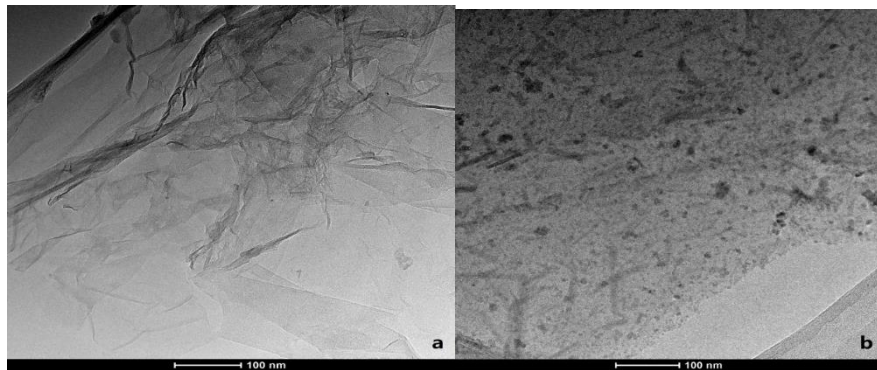
Fig. 1a shows a typical SEM image of AGO. The AGO possessed a sheet-like structure with a thin layer and a wrinkled edge. The obtained EDS image for AGO displayed some nitrogen doping. As shown in Fig. 1c, ball-like materials decorated and were anchored on the surface of the AGO layers. The composite was mainly composed of O, Fe, C, and N elements, based on the EDS of Fe<sub>3</sub>O<sub>4</sub>/AGO. It can be concluded that the Fe<sub>3</sub>O<sub>4</sub>/AGO composite had been successfully synthesized.





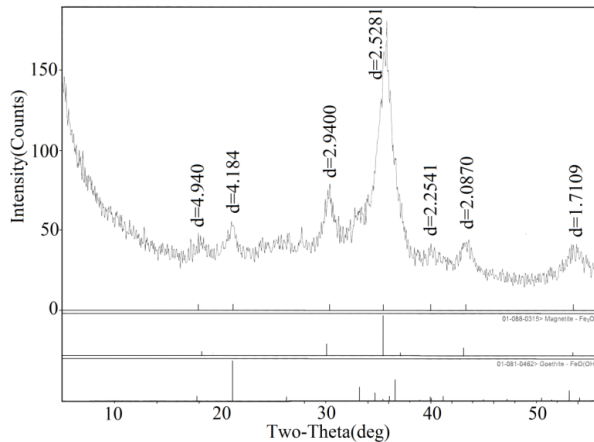
**Figure 1.** SEM of AGO (a) and Fe<sub>3</sub>O<sub>4</sub>/AGO (c) EDS of AGO (b) and Fe<sub>3</sub>O<sub>4</sub>/AGO (d)

Fig. 2 shows the TEM images of AGO and Fe<sub>3</sub>O<sub>4</sub>/AGO. Fig. 2a clearly shows a thin layer of AGO with some wrinkles across the surface. In Fig. 2b, it can be seen that a number of black Fe<sub>3</sub>O<sub>4</sub> particles cover the surface of AGO. This result was consistent with the XRD analysis of Fe<sub>3</sub>O<sub>4</sub>/AGO.



**Figure 2.** TEM images of AGO (a) and Fe<sub>3</sub>O<sub>4</sub>/AGO (b)

As shown in Fig. 3, the XRD of Fe<sub>3</sub>O<sub>4</sub>/AGO showed diffraction peaks at angles of 30.2°, 35.5°, 43.2° and 53.6°, corresponding to the cubic crystal phase of Fe<sub>3</sub>O<sub>4</sub> (JCPDS No. 75-0449). The diffraction peak at 2θ=20.5° can be attributed to FeOOH, indicating that the composite contains a small amount of FeOOH. The graphite oxide peak at 2θ=10.5° disappeared, indicating the successful transformation of graphite oxide into graphene. The XRD results showed that the composite contained a large amount of Fe<sub>3</sub>O<sub>4</sub> and a small amount of FeOOH. Fig. 3 also shows that the diffraction peaks are wide, which indicates that Fe<sub>3</sub>O<sub>4</sub>/AGO had a relatively small particle size.



**Figure 3.** XRD of  $\text{Fe}_3\text{O}_4/\text{AGO}$

Fig. 4 shows the electrocatalytic properties of different electrodes towards phenol. From Fig. 4e, it can be seen that there is an oxidation peak at 0.58 V, without a corresponding reduction peak, for the  $\text{Fe}_3\text{O}_4/\text{AGO}/\text{GCE}$ . This result shows that the electrocatalytic oxidation process for phenol is irreversible and that  $\text{Fe}_3\text{O}_4/\text{AGO}/\text{GCE}$  has a more obvious electrocatalytic performance compared with other electrodes. This may be due to the large specific surface area and good synergistic electrocatalytic properties of the  $\text{Fe}_3\text{O}_4/\text{AGO}$  nanocomposite.

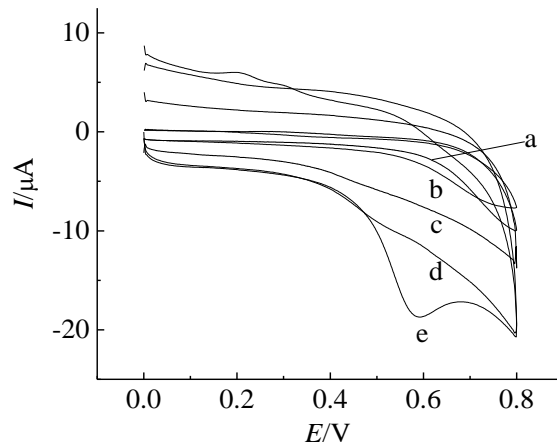


**Figure 4.** CVs for  $\text{Fe}_3\text{O}_4/\text{GCE}$  (a), GCE (b) and  $\text{AGO}/\text{GCE}$  (c) in the presence of 0.1mM phenol, for  $\text{Fe}_3\text{O}_4/\text{AGO}/\text{GCE}$  electrode in the absence (d) and presence (e) of 0.1mM phenol in 0.1 M PBS.

### 3.2 Effects of scan rates

The effects of scan rates on the electrochemical oxidation of phenol were studied on the  $\text{Fe}_3\text{O}_4/\text{AGO}/\text{GCE}$ . From Fig. 5a, it can be seen that the peak currents increased with increasing scan rates in the range of 0.04 to 0.14  $\text{V s}^{-1}$ . The anodic peak current ( $I_{\text{pa}}$ ) was proportional to the square root of the scanning rate ( $v^{1/2}$ ), which indicates a diffusion controlled process at the solution/electrode interface[26].

In addition, the anodic peak potential ( $E_{\text{pa}}$ ) was positively shifted with increasing scan rates,

indicating that the modified electrode could accelerate the electron transfer reaction and exhibited good electroactivity[27].  $E_{pa}$  was linear with the natural logarithm of the scanning rate ( $\lg v$ ) (Fig. 5c). The linear regression equation was  $E_{pa} = 0.066181\lg v + 0.6664$  ( $R=0.9945$ ). For completely irreversible electrode processes, the relationship between  $E_{pa}$  and  $\lg v$  can be expressed as follows [28]:

$$E_p = E^0 + [2.303RT/(anF)]\lg[RTk^0/(anF)] + [2.303RT/(anF)]\lg v \quad (1)$$

where  $\alpha$  is the transfer coefficient,  $k^0$  is the standard rate constant of the reaction,  $n$  is the electron transfer number,  $E^0$  is the formal redox potential and  $R$ ,  $T$  and  $F$  have their usual meanings. From the slope of the regression equation between  $E_p$  and  $\log v$ ,  $an$  can be calculated to be 0.8934. According to Bard and Faulkner [29],  $\alpha$  can be calculated from the following equation (2):

$$\alpha = \frac{47.7}{(E_p - E_{p/2})\text{mV}} \quad (2)$$

where  $E_{p/2}$  is the potential when the current is half that of the peak current. Thus,  $\alpha$  can be calculated to be 0.5963. Therefore, the electron transfer number,  $n$ , in the electrochemical oxidation of phenol can be calculated to be approximately 2, which demonstrates that the rate-limiting step was a two-electron transfer process.

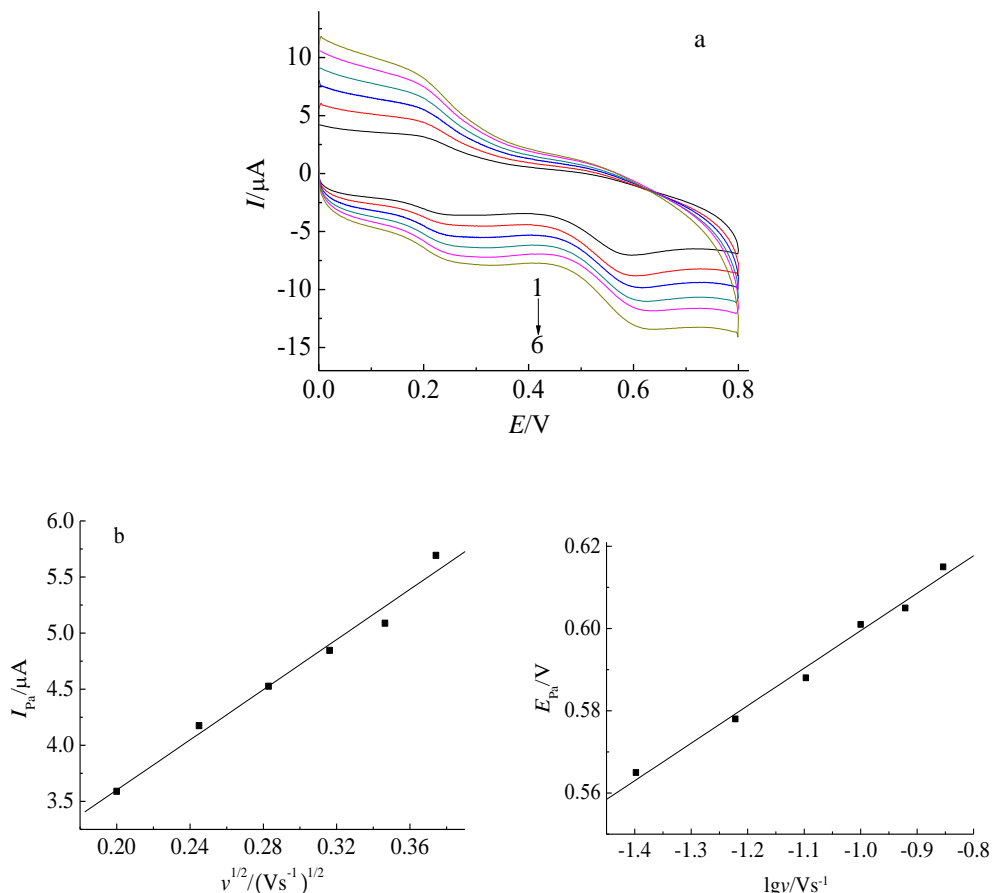


**Figure 5.** (a) CVs of  $\text{Fe}_3\text{O}_4/\text{AGO}/\text{GCE}$  in 0.1M PBS containing 0.1mM phenol at different scan rates (from Curve 1 to 6: 40, 60, 80, 100, 120 and 140  $\text{mV s}^{-1}$ ); (b) The plot of electrocatalytic peak current of phenol versus  $v^{1/2}$ ; (c) The plot of  $E_{pa}$  versus  $\log v$ .

### 3.3 Effects of pH

The effects of pH on the electrocatalytic oxidation of phenol were investigated. The results show that the peak current of the oxidation peak changed with changing pH and reached its maximum at pH 9.78 (Fig. 6A). Therefore, pH 9.78 was chosen for use in further studies, which could contribute to reducing the interference of metal cations.  $E_{pa}$  negatively shifted with increasing pH, indicating that protons were involved in the electrochemical reaction. Fig. 6B shows the relationship between  $E_{pa}$  and pH, which had the linear equation  $E_{pa}=1.051-0.0494 \text{ pH}$  ( $R=0.9828$ ). The slope of  $49.4 \text{ mV pH}^{-1}$  was close to the theoretical value of  $57.6 \text{ mV pH}^{-1}$ , indicating that an equal number of protons and electrons participated in the electrochemical reaction [30-32]. Therefore, the electrocatalytic oxidation of phenol on the surface of  $\text{Fe}_3\text{O}_4/\text{AGO}/\text{GCE}$  was a two-electron and two-proton process, and the electrocatalytic mechanism is shown in Equation 3, which is consistent with that found in the literature [33].

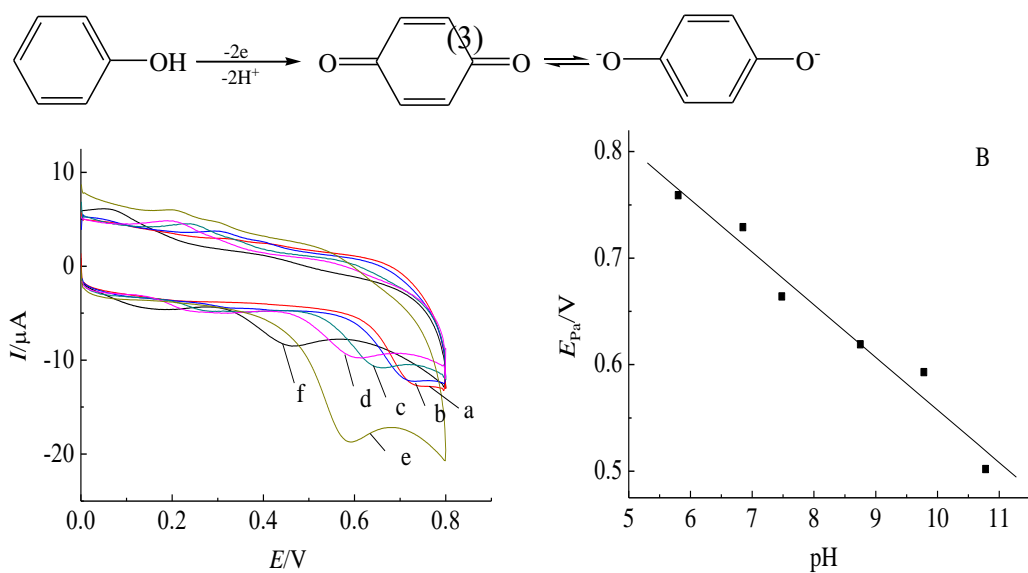


**Figure 6.** (A) CVs of  $\text{Fe}_3\text{O}_4/\text{AGO}/\text{GCE}$  in  $0.1\text{mM}$  phenol at different pH: (a) 5.80, (b) 6.85, (c) 7.48, (d) 8.75, (e) 9.78, (f) 10.78; (B) The plots of  $E_{pa}$  versus pH.

### 3.4 The determination of phenol

The concentration of phenol was determined by using linear sweep voltammetry (LSV). The results are shown in Fig. 7a. The linear equations between the oxidation peak current and the concentration of phenol were  $I_{pa} = 3.0119 + 127.8C$  ( $R=0.9984$ ) in the range of  $0.45 \mu\text{M}$  to  $56 \mu\text{M}$  and  $I_{pa} = 11.65205 + 48.55C$  ( $R=0.9949$ ) in the range of  $156 \mu\text{M}$  to  $556 \mu\text{M}$  with a lower detection limit of  $0.4 \mu\text{M}$  ( $S/N=3$ ).

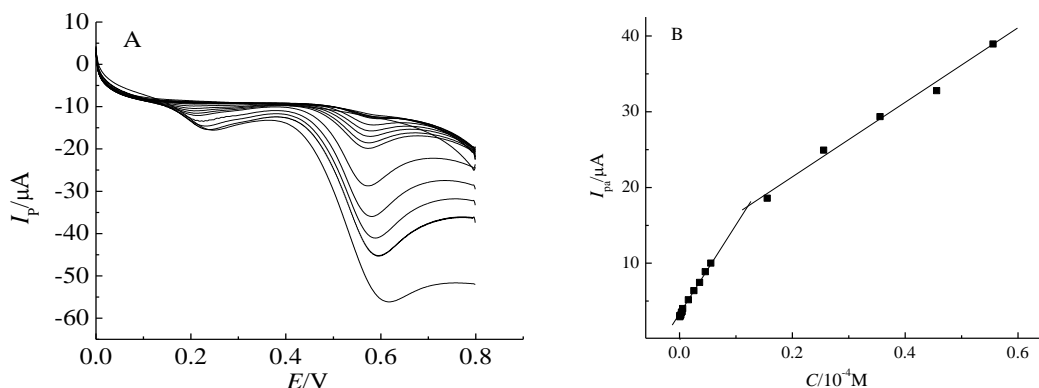


**Figure 7.** (A) The LSV obtained on the  $\text{Fe}_3\text{O}_4/\text{AGO}/\text{GCE}$  in 0.1 M PBS with different phenol concentration at  $0.1 \text{ V s}^{-1}$ ; (B) The plot of peak currents versus phenol concentration.

Comparisons among various efficient phenol sensors are shown in Table 1. Our method had either a lower detection limit or wider linear range than those of the previously reported sensors [32, 34-40].

**Table 1.** Comparison among different phenol sensors for the determination of phenol

Electrode	Linear range / $\mu\text{M}$	Detection limit / $\mu\text{M}$	Reference
Poly(zincon) /CPE	21-292, 357-922	9.0	29
CNT/PPy/HRP <sup>a</sup>	16-44	3.52	34
SBP/CPE <sup>b</sup>	50-700	50	35
GCE	11-100, 200-1000	11	36
Layered PANI sheets electrode	20-80	4.43	37
Tyrosinase-MWCNTa/SPE <sup>c</sup>	2.5-75	1.35	38
Tyrosinase-BiNPsc/SPE <sup>d</sup>	0.2-71	0.2	39
Tyrosinase-ZnO nanorods/Au	0.6-20	0.6	40
$\text{Fe}_3\text{O}_4/\text{AGO}/\text{GCE}$	0.45-56, 156-556	0.4	This work

a:carbon nanotube-poly(pyrrole)-horseradish peroxidase nano-bioccomposite film. b: soybean peroxidase modified carbon paste electrodes. c: screen-printed electrode. d: bismuth nanoparticles.

### 3.5 Reproducibility, stability and anti-interference performance

The reproducibility, stability and anti-interference performance of the  $\text{Fe}_3\text{O}_4/\text{AGO}/\text{GCE}$  sensor

were evaluated. The current responses of six identically modified electrodes were studied in a 0.1 mM phenol solution, and the relative standard deviation (RSD) was 3.2%, which proves that the Fe<sub>3</sub>O<sub>4</sub>/AGO/GCE sensor has a high reproducibility. Ten successive measurements of a single electrode yielded an RSD of 3.8%, which shows that the sensor is stable and can be used for the repeated detection of phenol. At the same time, the long-term stability of the phenol sensor was also investigated. After 2 weeks, the current response to phenol was 89% of the original current response, indicating that the Fe<sub>3</sub>O<sub>4</sub>/AGO/GCE sensor was stable. The anti-interference performance of the sensor was studied in a 1.0 mM phenol solution. The results showed that, for an RSD of less than 5%, common cations and anions (Na<sup>+</sup>, K<sup>+</sup>, ClO<sub>4</sub><sup>-</sup>, Ni<sup>2+</sup>, Ca<sup>2+</sup>, Br<sup>-</sup>, Zn<sup>2+</sup>, Mg<sup>2+</sup>, SO<sub>4</sub><sup>2-</sup>, NO<sub>3</sub><sup>-</sup>, and NO<sub>2</sub><sup>-</sup>) at 100 times the concentration of phenol had no obvious interference in the detection of phenol.

### 3.6 Application for real sample analysis

The validity of the proposed method for phenol determination was evaluated. Fe<sub>3</sub>O<sub>4</sub>/AGO/GCE sensor was applied to determine phenol in oilfield wastewater, and the results were shown in Table 2. The results were satisfactory, indicating that Fe<sub>3</sub>O<sub>4</sub>/Ag/GCE sensor could be applied for real sample analysis.

**Table 2.** Detection results of phenol in oilfield wastewater samples using Fe<sub>3</sub>O<sub>4</sub>/AGO/GCE

No.	Measured /μM	phenol added /μM	phenol found <sup>a</sup> /μM	Recovery /%
1	5.12	20	25.32	101
2	6.08	40	46.75	102

(a. The result of average of three determinations by the sensor)

## 4. CONCLUSIONS

In this work, a sensitive electrochemical sensor for the detection of phenol was fabricated based on Fe<sub>3</sub>O<sub>4</sub>/AGO. Compared with other previously reported sensors for phenol detection, the proposed phenol sensor based on Fe<sub>3</sub>O<sub>4</sub>/AGO displayed a wider linear range and a lower detection limit due to the large surface area and good conductivity of the Fe<sub>3</sub>O<sub>4</sub>/AGO nanocomposite, which improved the electron transfer efficiency between the modified electrode and the phenols. The phenol sensor based on Fe<sub>3</sub>O<sub>4</sub>/AGO could also be applied to detect phenol in an oilfield wastewater sample with satisfactory results.

## ACKNOWLEDGMENTS

This work was financially supported by Shaanxi Provincial Natural Science Foundation (No. 2018JM2014) and Industrial research project of Science and Technology Department of Shaanxi Province (No. 2017GY-179).

## References

1. H.B. Lee, E.T. Peart, M.L. Svoboda, *J. Chromatogr. A*, 1094 (2005) 122.
2. R. Mateos, J.L. Espartero, M. Trujillo, J.J. Ríos, M. León-Camacho, F. Alcudia, A. Cert, *J. Agr. Food. Chem.*, 49 (2001) 2185.
3. W. Frenzel, J. Oleksy-Frenzel, J. Mörlen, *Anal. Chim. Acta*, 261 (1992) 253.
4. S. Morales, R. Cela, *J. Chromatogr. A*, 846 (1999) 401.
5. P. Stratil, B. Klejdus, V. Kubáň, *J. Agr. Food. Chem.*, 54 (2006) 607.
6. J. R. Sun, H. Y. Lu, H.B. Lin, L.L. Du, W.M. Huang, H.D. Li, T. Cui, *Sep. Purif. Technol.*, 88 (2012) 116.
7. H. Karimi-Maleh, M. Moazampour, A. Ensafi, S. Mallakpour, M. Hatami, *Environ. Sci. Pollut. R.*, 21 (2014) 5879.
8. F. Liu, Y.X. Piao, C.J. Seob, S.T Seok, *Biosens. Bioelectron.*, 50 (2013) 387.
9. M. Abaker, G.N. Dar, A. Umar, S.A. Zaidi, A.A. Ibrahim, S. Baskoutas, A. Al-Hajry, *Sci. Adv. Mater.*, 4 (2012) 893.
10. H.K. Seo, S. Ameen, M.S. Akhtar, H.S. Shin, *Talanta*, 104 (2014) 219.
11. J.F. Ping, J. Wu, Y.X. Wang, Y.B. Ying, *Biosens. Bioelectron.*, 34 (2012) 70.
12. V. Mani, A.P. Periasamy, S.M. Chen, *Electrochim. Commun.*, 17 (2012) 75.
13. N. Promphet, P. Rattanarat, R. Rangkupan, O. Chailapakul, N. Rodthongkum, *Sensor. Actuat. B-Chem.*, 207 (2015) 526.
14. X.L. Ye, Y.L. Du, D.B. Lu, C.M. Wang, *Anal. Chim. Acta*, 779 (2013) 22.
15. G.B. Yang, L.L. Li, R.K. Rana, J.J. Zhu, *Carbon*, 61 (2013) 357.
16. J. Luo, S.S. Jiang, H.Y. Zhang, J.Q. Jiang, X.Y. Liu, *Anal. Chim. Acta*, 709 (2012) 47.
17. M.L. Chen, H.J. He, X.W. Chen, J.H. Wang, *Langmuir*, 28 (2012) 16469.
18. Y.T. Liu, Y.Li, Y. Wei, *J. Sep. Sci.*, 37 (2014) 3745.
19. Y.H. Ma, Z.Y. Zhang, C.L. Ren, G.Y. Liu, X.G. Chen, *Analyst*, 137 (2012) 485.
20. Y.L. Yang, Y. You, Y.C. Liu, Z.S. Yang, *Microchim. Acta*, 180 (2013) 379.
21. J.Y. Qu, Y. Dong, T.F. Lou, X.P. Du, *Anal. Lett.*, 47 (2014) 1797.
22. C.C. Chu, L. Li, S. Li, M. Li, S.G. Ge, J.H. Yu, M. Yan, X.R. Song, *Microchim. Acta*, 180 (2013) 1509.
23. W.S.H. Jr, R.E. Offeman, *J. Am. Chem. Soc.*, 80 (1958) 1339.
24. H.A. Becerril, J. Mao, Z. Liu, R.M. Stoltenberg, Z. Bao, Y. Chen, *Acs. Nano*, 2 (2008) 463.
25. C. Z. Zhang, R. Hao, H.B. Liao, Y.L. Hou, *Nano Energy*, 2 (2013) 88.
26. H.M. Moghaddam, H. Beitollahi, S. Tajik, M. Malakootian, H. K. Maleh, *Environ. Monit. Assess.*, 186(2014) 7431.
27. M. Hasanzadeh, M. H. Pournaghi-Azar, N. Shadjou, A. Jouyban, *RSC Adv.*, 4(2014) 51734.
28. E. Laviron, *J. Electroanal Chem.*, 101 (1979) 19.
29. A.J. Bard, L.R. Faulkner, *Electrochemical Methods Fundamentals and Application*. 2nd ed., Wiley 2004, 236.
30. H. S. Yin, L. Cui, Q. P. Chen, W. J. Shi, S. Y. Ai, L. S. Zhu, L. N. Lu, *Food. Chem.*, 125 (2011) 1097.
31. H.B. Li, J. Li, D.M. Meng, J.Y. Peng, Q.J. Qiao, Z.J. Yang, Q. Xu, X.Y. Hu, *Sci. China Chem.*, 54(2011) 1116.
32. W.L. Qin, X. Liu, H.P. Chen, J. Yang, *Anal. Methods-UK*, 6(2014)5734.
33. J.L. Boudenne, O. Cerclier, J. Galéa, E.V.D. Vlist, *Appl.Catal. A*, 143(1996 )185.
34. S. Korkut, B. Keskinler, E. Erhan, *Talanta*, 76 (2008) 1147.
35. A.S. Bassi, C. McGrath, *J. Agr. Food Chem.*, 47 (1999) 322.
36. L. Fotouhi, M. Ganjavi, D. Nematollahi, *Sensors-Basel.*, 4 (2004) 170.
37. H.K. Seo, S. Ameen, M.S. Akhtar, H.S. Shin, *Talanta*, 104 (2013) 219.
38. M. Guix, B. P. Lopez, M. Sahin, M. Roldan, A. Ambrosia and A. Merkoc, *Analyst*, 135 (2010)

1918.

39. C.C. M. Martinez, M. Cadevall, M. Guix, J. Ros, A. Merkoci, *Biosens. Bioelectron.*, 40 (2013) 57.
40. B.X. Gu, C.X. Xu, G.P. Zhu, S.Q. Liu, L.Y. Chen, X.S. Li, *J. Phys. Chem. B*, 113 (2009) 377.

© 2019 The Authors. Published by ESG ([www.electrochemsci.org](http://www.electrochemsci.org)). This article is an open access article distributed under the terms and conditions of the Creative Commons Attribution license (<http://creativecommons.org/licenses/by/4.0/>).